Philip Schantl and Christian Majcenovic

Reaction Textures in Al$_2$O$_3$–SiO$_2$ Bricks Induced by Gaseous SO$_x$ Attack: New Insights From Mineralogy and Thermodynamic Modelling

In the sulphate process, Al$_2$O$_3$-SiO$_2$ refractory bricks are used to line rotary kilns. During calcination of hydrated TiO$_2$, these bricks are subjected to highly aggressive and corrosive SO$_x$ gas attack at operating temperatures between 850–950 °C. A systematic mineralogical study on mineral reaction textures and compositional zoning from the hot face towards the cold end of a representative used fireclay brick in combination with thermochemical modelling and the application of the Dietzel's field strength enabled the thermochemical modifications of the brick microtexture and the acting wear mechanisms to be reconstructed. Gaseous SO$_x$ supply resulted in a strong alteration of the mullite dominated brick matrix up to a depth of ~28 mm from the immediate hot face through mullite decomposition and aluminium sulphate plus quartz forming reactions. Based on thermochemical calculations these reactions appear between 760 and 440 °C. In a second step, the newly formed aluminium sulphate decomposed and transformed to flaky corundum by SO$_x$ gas releasing reactions. This could only be observed at the very hot face of the brick, up to a depth of ~10 mm, where minimum temperatures of 720–780 °C were reached. These temperature estimations were obtained by the combined application of thermochemical phase equilibrium and reaction delta G^0 calculations. This two-step corrosion texture development led to a significant weakening of the brick bonding structure and enabled consequent discontinuous material loss at the refractory hot face by abrasive wear during the feed material transport through the rotary kiln. As a result of the postmortem study, a special silica-sol impregnation is recommended to improve the resistance of the brick matrix against volatile SO$_x$ attack.

Introduction

The usage of concentrated sulphuric acid during the production of highly pure TiO$_2$ pigment challenges refractory producers because products lining the rotary kiln used to calcine hydrated TiO$_2$ must withstand highly aggressive and corrosive SO$_x$ gas. To resist such a gas attack, SiO$_2$-rich fireclay bricks are preferentially used to line these kilns, as silicon is known to have a high resistance against sulphur attack. This is deduced from the Dietzel's field strength which indicates that both silicon and sulphur have a high field strength of 1.56 Å^{-2} and 2.60 Å^{-2}, respectively [1], and thus have a low affinity for each other to form a new binary oxidic compound. However, aluminium within these fireclay bricks is much lower in the Dietzel's field strength (0.84 Å^{-2}) than silicon and has a high potential to interact with acidic SO$_x$ gas to form new phases that can destruct and weaken the microtexture of the bricks' hot face. As a result, the refractory product is vulnerable to mechanical wear and mass loss by abrasion.

In this study, new insights into the microtextural and microchemical modification and the consequent wear phenomena of a fireclay brick that was used in a TiO$_2$ rotary kiln are presented. These findings are based on detailed microscopic observations of mineral reaction textures, the measured compositional zoning from the hot face towards the cold end of the investigated brick, and thermochemical phase equilibrium modelling. In addition, a solution that improves the bricks' resistance against volatile SO$_x$ gas attack to avoid microtextural modifications is provided.

Sulphate Process

Due to its whiteness, high refractive index, and resulting light-scattering ability, TiO$_2$ is commonly used for whitening papers, paints, rubbers, plastics, and other materials. Since the early twentieth century, this pigment can be produced commercially by the sulphate process [2–5]; a batch process where finely ground ilmenite or high-TiO$_2$ slag is digested in concentrated sulphuric acid. After initial heating, a strong exothermic reaction (+220 °C) starts between the titanium-bearing raw material and the acid. This leads to the formation of a porous solid cake which is then dissolved in diluted acid and water to yield a titanyl sulphate + iron sulphate solution according to the equation:

$$FeTiO_3 + 2\ H_2SO_4 \rightarrow TiOSO_4 + FeSO_4 + 2\ H_2O \qquad (1)$$

By adding scrap iron, any ferric iron present is reduced to the ferrous state to avoid any precipitation of embrowning ferric iron during the following process steps and to facilitate washing of the titanium-bearing material, as ferric iron is less absorbing than ferrous iron. This reduction step is not necessary when high-TiO$_2$ slag is used as feed material since low amounts of iron in the slag are already in a reduced state. To remove any unreacted solids after the reduction of ferrous iron, the solution is clarified by filtration and settling. Ferrous sulphate heptahydrate, which crystallises from the iron sulphate, is then filtered out from the solution.

After iron removal, the solution is concentrated and titanyl sulphate is hydrolysed (at 95–110 °C) to hydrated TiO_2 according to the equation:

$$TiOSO_4 + 2 H_2O \rightarrow TiO_2 \cdot n\, H_2O + H_2SO_4 \qquad (2)$$

In a final step, the hydrated TiO_2 is calcined in a rotary kiln to precipitate rutile or anatase. This calcination needs temperatures in the range of 850–950 °C. A representative image of the interior of a fireclay brick lined rotary kiln is presented in Figure 1.

Methods

After furnace shut down, a worn clay-bonded fireclay brick was taken from the rotary kiln for a postmortem study at RHI Magnesita's Technology Center Leoben (Austria). The investigation aim was to provide information about the condition of the refractory, the wear mechanism, and possible optimisation potential. Firstly, a visual inspection was conducted on the worn brick and its cross-section. Succeeding detailed mineralogical investigations and quantitative mineral analyses were carried out on two polished sections prepared from the hot face area using a reflected light microscope and a JEOL JSM-6460 scanning electron microscope (SEM) equipped with an Oxford X-Max 100 energy dispersive system (EDS) and an Oxford wavelength dispersive system. Additional high-resolution, back-scattered electron (BSE) images were obtained from a JEOL JSM-7900F field emission gun SEM. Measurement conditions of the SEM were a 20 kV acceleration voltage, 2 nA beam current, and ~1 µm beam diameter. Natural and synthetic mineral standards were used for element calibration.

In order to evaluate the chemical modification and penetration of corrosive species into the brick matrix from the hot face towards the cold end, an ~38 mm long "semi-quantitative" compositional profile was obtained by measuring twenty-five 1.5 x 1.5 mm EDS matrix area analyses within the two prepared polished sections.

Postmortem Study

On visual inspection (Figure 2), the investigated clay-bonded fireclay brick showed a crumbly hot face area up to a depth of ~4 cm. The surface was rough and irregular which pointed to discontinuous mass loss.

Three zones labelled with A, B, and C had developed from the hot face towards the cold end of the worn brick. These zones differed in their colouration and textural appearance. While zone A and B were friable, zone C appeared widely dense and compact.

Microscopy and Mineral Chemistry

Zone A

Based on the mineralogical compositions, zone A could be subdivided into zone A1 and A2. In zone A1, comprising the very first 5 mm from the immediate hot face, fireclay coarse grains showed patchy, granular rim areas (Figure 3a) which were strongly enriched in SiO_2 and depleted in Al_2O_3 (Figures 3c and 3d). The inner parts of these fireclay grains appeared widely unaltered and consisted of the original assemblage mullite and glassy phase. The former mullite dominated matrix was entirely modified. It appeared porous and was defined by abundant newly formed tiny corundum plates, up to 4 µm in size (Figure 3b). SiO_2 disappeared completely within the matrix (Figure 3d).

In zone A2, from a depth of ~5 mm to ~10 mm, it was similar to zone A1 but showed the additional occurrence of rare aluminium sulphate within the corundum dominated matrix (Figures 3e and 3f). Typically, this aluminium sulphate showed decomposition features on its crystal boundaries and was partly replaced by tabular corundum crystals on its edges.

Figure 1.

Representative photograph of the interior area of a fireclay brick lined rotary kiln used for the calcination of hydrated TiO_2 to precipitate rutile or anatase.

Figure 2.

Photograph of the worn clay-bonded fireclay brick showing a rough hot face and three distinct zones (A, B, and C). Polished sections for microscopy were taken from the black box (M). The compositional EDS profile line from zone A towards zone C is indicated as a grey arrow labelled P.
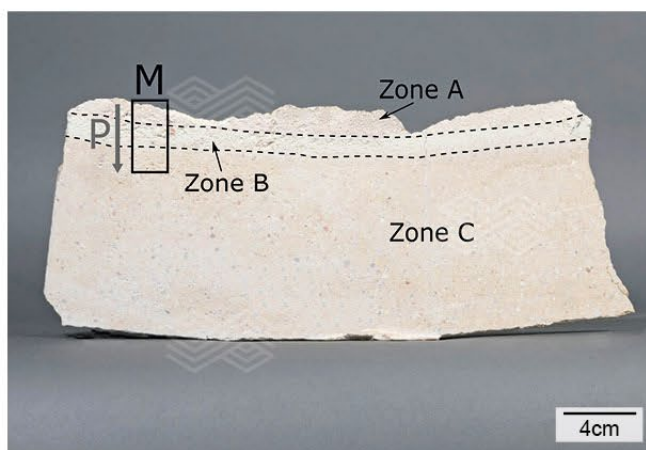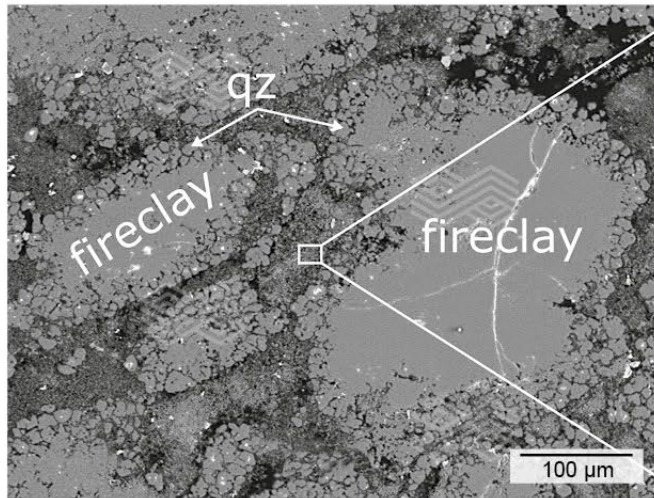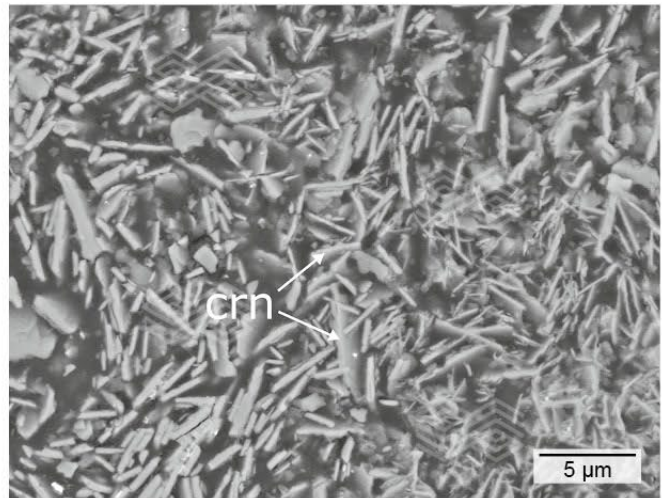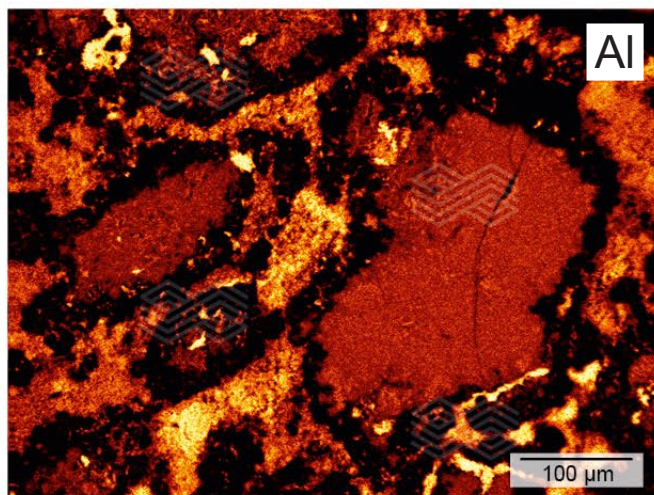
Figure 3.

BSE images and X-ray element distribution mappings of zone A. (a) fireclay coarse grains with a patchy, granular rim area consisting of quartz (qz). (b) the matrix appears porous and is composed of tiny tabular corundum (crn) crystals. (c, d) X-ray element distribution mappings of Al and Si indicate that the rim area of the fireclay coarse grains is strongly depleted and enriched in Al and Si, respectively. (e) aluminium sulphate occurs rarely within the brick matrix in a thin layer in zone A, near to zone B. (f) the matrix within this thin layer in zone A is mainly composed of tiny tabular corundum (crn) crystals.
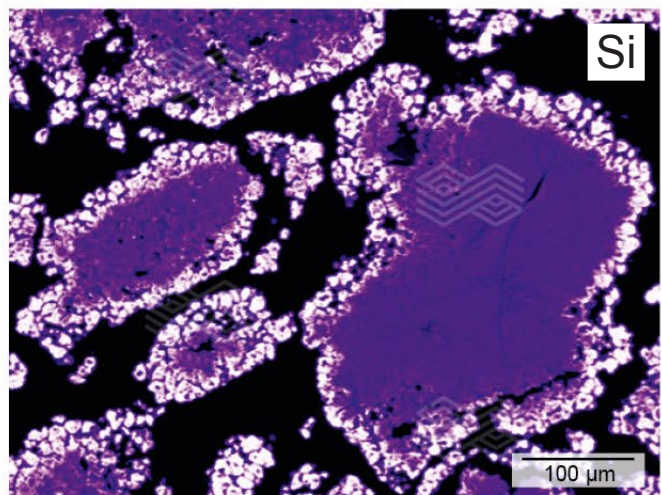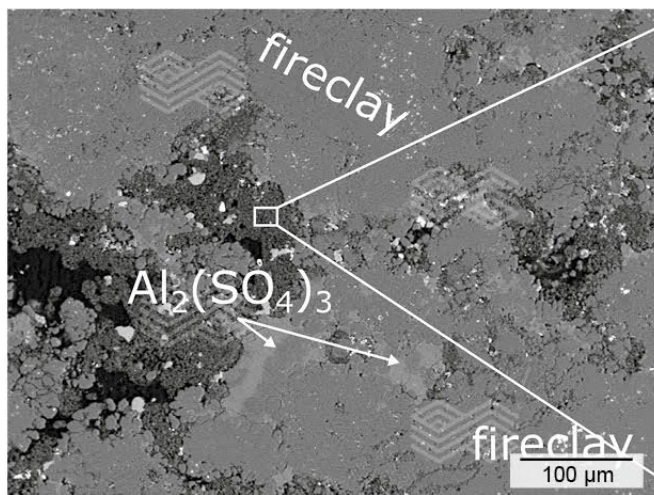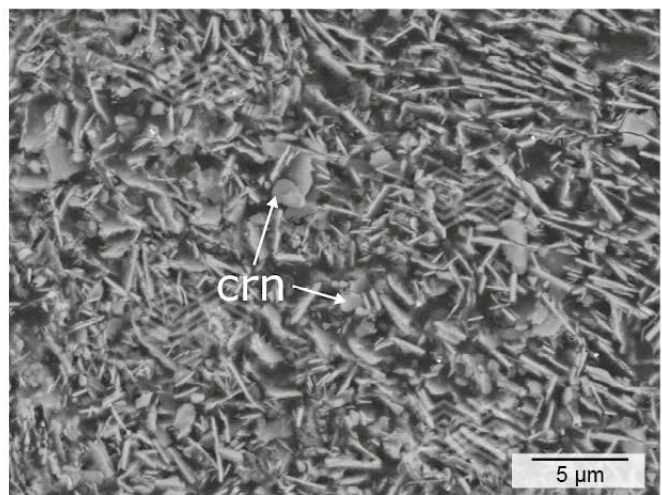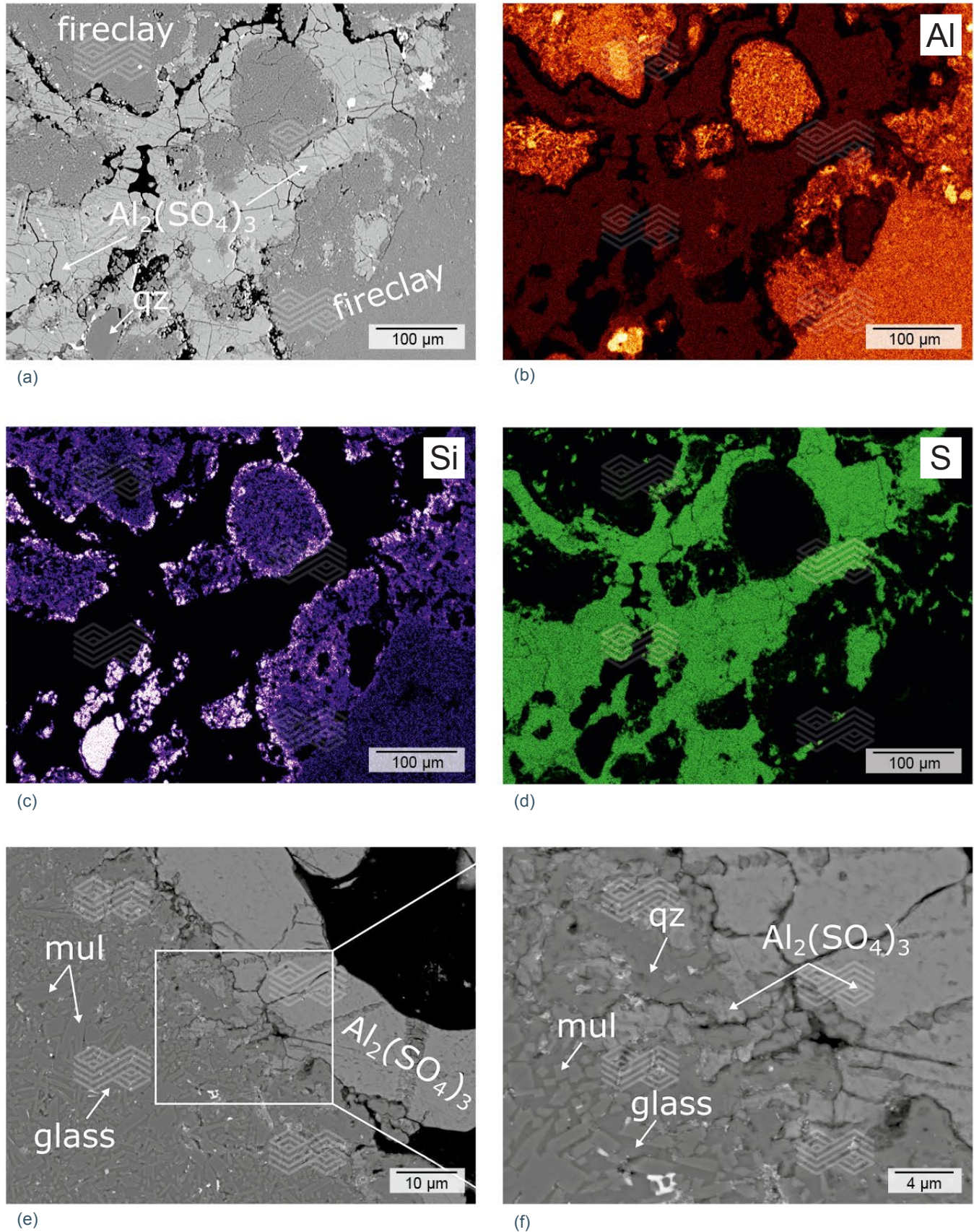
Figure 4.

BSE images and X-ray element distribution mappings of zone B. (a) fireclay coarse grains show an altered rim area and are surrounded by pores. The matrix is totally modified and consists of newly formed aluminium sulphate and minor quartz (qz). No primary mullite (mul) can be found within this matrix. (b–d) X-ray element distribution mappings of Al, Si, and S show that the rim of the fireclay coarse grains is strongly depleted in Al and enriched in Si. The matrix consists of high S and moderate Al concentrations. No primary Si can be found within this matrix. (e, f) primary mullite (mul) crystals at the edges of fireclay coarse grains are decomposed to form aluminium sulphate and quartz (qz).

Zone B

Fireclay coarse grains in zone B showed similar textural and chemical features as in zone A. The rim areas were modified and had high SiO_2 and low Al_2O_3 concentrations (Figure 4). The central part was unaffected by chemical and textural modifications and consisted of primary mullite and glassy phase. These fireclay grains were embedded within a strongly altered matrix that mainly consisted of newly formed aluminium sulphate and minor quartz (Figure 4a). Typically, the aluminium sulphate was highly pure and contained low Fe_2O_3 (0.74–1.19 wt.%), MgO (0.34–0.57 wt.%), and Na_2O (<0.52 wt.%) concentrations (Table I). Based on mineral formula calculations, these phases could be identified as millosevichites.

Aluminium sulphate was found locally with high K_2O concentrations in the range of 15.98–16.20 wt.% (see Table I) and was determined to be yavapaiite. High-resolution BSE images of the interface area between fireclay grains and aluminium sulphate revealed that primary mullite crystals of fireclay grains had decomposed into aluminium sulphate and quartz (Figures 4e and 4f).

Zone C

No textural or chemical alterations could be found in zone C of the studied brick. Fireclay coarse grains consisted of primary mullite and glassy phase. They occurred within an unaltered fine-grained matrix composed of small mullite crystals and interstitial glassy phase.


Semi-Quantitative Compositional Profile

The compositional matrix profile from the immediate hot face up to ~38 mm depth (Figures 2 and 5) showed a strong correlation between changes of the Al_2O_3, SiO_2, and SO_3 contents, which fitted with the mineralogical observations.

The very first ~5 mm of zone A1 were characterised by high Al_2O_3 (30–40 wt.%), low SiO_2 (<10 wt.%), and even lower SO_3 (<4 wt.%) concentrations. In zone A2, from a depth of ~5 to ~10 mm, Al_2O_3 started to decrease, while SiO_2 and SO_3 showed a slight increase. At ~10 mm from the immediate hot face, SO_3 showed a sharp and pronounced increase and marked the onset of zone B. The following 18 mm of the profile were highly enriched in SO_3 with varying contents between 30 and 45 wt.%. SiO_2 and Al_2O_3 was generally low in this zone and showed a strong fluctuation at <20 wt.%. At ~28 mm depth, zone B had a sharp and pronounced depletion of SO_3 and a coincident increase of Al_2O_3 and SiO_2. The following zone C showed a SO_3 concentration close to 0 wt.% and constant Al_2O_3 and SiO_2 concentrations at ~36 and ~49 wt. %, respectively. This indicated a chemically unaltered fireclay matrix.

Figure 5.

Compositional matrix profile from the immediate hot face of the investigated worn fireclay brick up to a depth of ~38 mm. A strong correlation between changes of the Al_2O_3, SiO_2, and SO_3 contents can be observed.
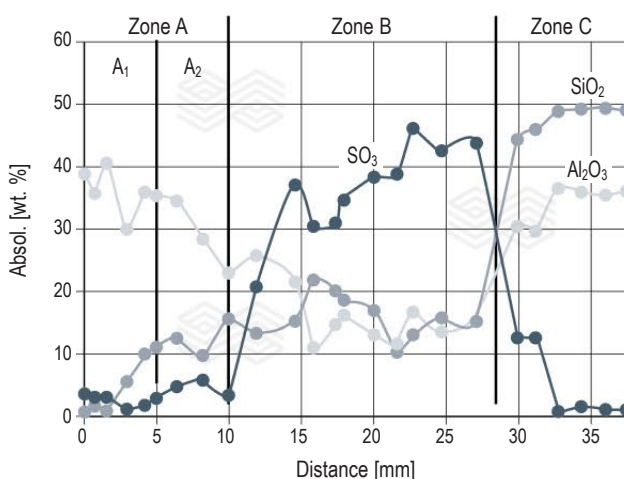
Table I.

Representative composition of aluminium sulphates within the matrix of zone B. Abbreviations include below detection (b.d.).

| [wt.%]	Millosevichite						Yavapaiite			
SO_3	70.06	68.74	69.78	69.39	69.19	68.12	61.98	61.87	62.14	60.94
Al_2O_3	28.82	29.52	29.37	29.13	28.76	29.29	19.58	19.36	20.37	19.10
Fe_2O_3	1.10	0.84	0.74	0.77	1.19	1.07	1.14	1.40	1.40	0.89
MgO	0.57	0.34	0.36	b.d.	0.70	0.44				
Na_2O	0.44	b.d.	b.d.	0.33	0.52	0.29	0.84	0.85	0.90	1.14
K_2O							16.20	16.00	15.98	16.02
Total	**100.99**	**99.44**	**100.25**	**99.62**	**100.36**	**99.21**	**99.74**	**99.48**	**100.79**	**98.09**
	Atoms per 12 O						Atoms per 8 O			
S	2.987	2.970	2.983	2.991	2.974	2.959	1.994	1.996	1.979	1.996
Al	1.907	2.003	1.983	1.972	1.942	1.998	0.989	0.981	1.019	0.983
Fe^{3+}	0.047	0.036	0.032	0.033	0.051	0.047	0.037	0.045	0.045	0.029
Mg	0.048	0.029	0.031		0.060	0.038	0.070	0.071	0.074	0.096
Na	0.048			0.037	0.058	0.033				
K							0.886	0.877	0.865	0.892
Σ Cations	**5.037**	**5.038**	**5.029**	**5.033**	**5.085**	**5.075**	**3.976**	**3.970**	**3.982**	**3.996**

Phase Equilibrium Modelling

In order to gain additional information about the gas attack and corrosive reactions in zone A and B of the studied worn brick, thermochemical phase equilibrium diagrams based on the observed mineral textures and newly formed phases were constructed. The Gibbs free energy minimisation software FactSage [6,7] was used, employing the thermodynamic datasets FactPS, FToxide, and FTmisc.

Reconstruction of Gas Species Attacking the Refractory

The high abundance of aluminium sulphate in zone B implies a supply of SO_x gas and its interaction with the refractory material. It is therefore reasonable to assume that remnants of liquid H_2SO_4 from either the dissolution procedure (equation 1) or the hydrolysis step (equation 2) were dragged into the rotary kiln where it evaporated to gaseous SO_x species at operating temperatures of 850–950 °C. To estimate the relative quantities of acting SO_x gas species in this temperature range, the phase stabilities of 1 mole H_2SO_4 from 0–1000 °C were modelled. The computed diagram is shown in Figure 6 and indicates that liquid H_2SO_4 changes to gaseous species at about 310 °C. From ~310 to ~500 °C the gaseous H_2SO_4 shows a pronounced dissociation according to the equation:

$$H_2SO_4 \text{ (g)} \rightarrow SO_3 \text{ (g)} + H_2O \text{ (g)} \tag{3}$$

This leads to a pronounced decrease of H_2SO_4 (g) and a significant increase of SO_3 (g) species, while H_2O (g) increases moderately. At ~500 °C the dissociation reaction changes and SO_3 (g) starts to decompose generating SO_2 (g) and O_2 (g) as follows:

$$SO_3 \text{ (g)} \rightarrow SO_2 \text{ (g)} + 0.5 \, O_2 \text{ (g)} \tag{4}$$
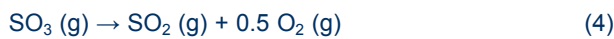
Based on the computed stabilities of sulphur-bearing species (see Figure 6), relatively high SO_2 (g) and low SO_3 (g) concentrations that interact with the refractory material at operating temperatures of 850–950 °C during the calcination of hydrated TiO_2 can be assumed. In addition, the presence of H_2O (g) and O_2 (g) is given.

Figure 6.

Phase stabilites of 1 mole H_2SO_4 from 0–1000 °C, computed by FactSage.

(3) H_2SO_4 (g) $\rightarrow SO_3$ (g) + H_2O (g)   (4) SO_3 (g) $\rightarrow SO_2$ (g) + 0.5 O_2 (g)
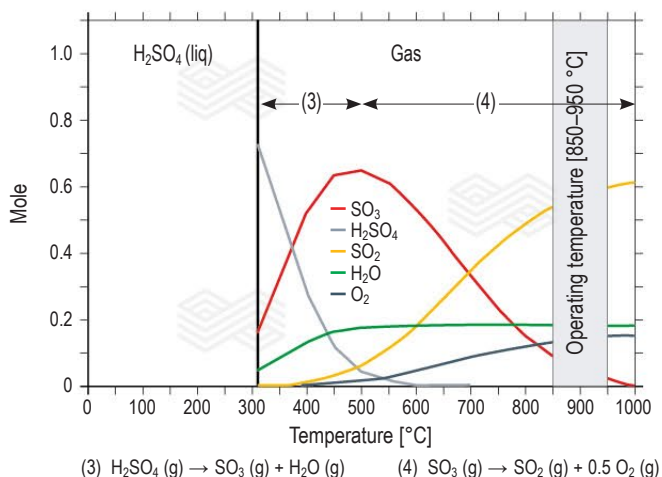
Temperature Estimation of Acting Corrosive Reactions in Zone A

Although the matrix of zone A was defined by a pervasive mineralogical and microtextural alteration, microscopic observations (see Figure 3) in combination with a semi-quantitative chemical profile (see Figure 5) indicated the formation of abundant small corundum plates at the expense of previously stable aluminium sulphate via SO_x (g) releasing reactions. Assuming a pure aluminium sulphate end member (millosevichites, see Table I), the following temperature driven equations can be formulated as responsible for the mineralogical observations in zone A:

$$Al_2(SO_4)_3 \rightarrow Al_2O_3 + 3 \, SO_3 \tag{5}$$

$$Al_2(SO_4)_3 \rightarrow Al_2O_3 + 3 \, SO_2 + 1.5 \, O_2 \tag{6}$$

To obtain meaningful temperature estimates for these reactions, the phase stabilities of 1 mole $Al_2(SO_4)_3$ over the temperature range of 300–1000 °C were performed. The resulting diagram is shown in Figure 7a. Accordingly, aluminium sulphate appears up to temperatures of 722 °C. Corundum, which was observed as a stable phase in zone A, occurs at temperatures higher than 722 °C in the presence of gaseous SO_3, SO_2, and O_2. The amounts of SO_2 and O_2 show an increase from 722 °C to 1000 °C, which correlates with a SO_3 decrease. This is due to the progressive SO_3 dissociation with increasing temperature. Additional temperature restrictions were achieved by calculating delta G^0 for equations 5 and 6 from 300–1000 °C (Figure 7b). It can be seen that delta G^0 of both reactions decreases with increasing temperature. This confirms the raising tendency of corundum formation due to aluminium sulphate decomposition with increasing temperatures. It also shows that delta G^0 reaches 0 Joule at 780 °C. Thus, a minimum of 780 °C can be assumed for the corundum formation in zone A according to equations 5 and 6. This is about 60 °C higher than the minimum temperatures obtained from the phase stability diagram in Figure 7a, as only the pure end member reactions were considered.

Temperature Estimation of Acting Corrosive Reactions in Zone B

Based on the observed microtextures, mullite within the brick matrix and fireclay rims decomposed to form aluminium sulphate and quartz in the presence of SO_x gas (Figures 4a, 4e, and 4f). Assuming pure end members, two equations can be postulated to explain these textures:

$$Al_6Si_2O_{13} + 9 \, SO_3 \rightarrow 3 \, Al_2(SO_4)_3 + 2 \, SiO_2 \tag{7}$$

$$Al_6Si_2O_{13} + 9 \, SO_2 + 4.5 \, O_2 \rightarrow 3 \, Al_2(SO_4)_3 + 2 \, SiO_2 \tag{8}$$

Using the stoichiometry of these reactions (e.g., 1 mole $Al_6Si_2O_{13}$ and 9 mole SO_3), the phase stabilities from 300–1000 °C were computed to estimate the temperature dependent stability of mullite in the presence of SO_x gas (Figure 7c). It shows that mullite is stable at temperatures higher than 760 °C and decomposes from 760–440 °C to form aluminium sulphate and quartz.

At temperatures lower than 440 °C only aluminium sulphate and quartz appear. Based on these calculations, the formation of the observed phase assemblage aluminium sulphate + quartz at the expense of mullite can only be formed in the temperature range of 760–440 °C. This was also confirmed by the delta G^0 calculations for equations 7 and 8 over the temperature range of 300–1000 °C (Figure 7d). There, it shows that delta G^0 of both reactions decreases with decreasing temperatures, which implies that mullite decomposition in the presence of SO_x is intensified with decreasing temperatures. As delta G^0 of both reactions reaches 0 Joule at 760 °C, it is estimated that equations 7 and 8 occur at temperatures lower than 760 °C.

Aluminium Sulphate Formation Explained by the Application of Dietzel's Field Strength

The tendency of new compounds to form from a refractory and externally supplied chemical species depends on the difference in their basicity/acidity, which was first described by Adolf Dietzel in 1948. In order to quantify the basicity/acidity of a single species, he defined the so-called Dietzel's field strength (Fs). It is expressed through the equation:

$$Fs = Zc/a^2 \qquad (9)$$

Where Zc is the valence of the cation and a is the distance in Å between the cation and the bonded oxygen.

This approach is based on the bonding strength due to the Coulomb force (attraction/repulsion) between cations and anions in a liquid glass [8]. Accordingly, elements with a high Fs are defined as acidic and elements with a low Fs are defined as basic species.

The field strength difference (ΔFs) between two species gives indications about their tendency to form a binary oxidic compound. In this respect, a minimum ΔFs of 0.3 Å^{-2} is needed to form a new compound and the higher the difference between two species, the higher the tendency of new compound formation. If the Fs of two species is similar and ΔFs is lower than 0.3 Å^{-2}, no compound formation will occur [8].

In the present study, the refractory compound mullite was found to strongly interact with externally supplied SO_x gas species to form the new binary oxidic compound aluminium sulphate and remnant quartz (Figure 4a). This interaction can be considered in terms of the respective cation's Dietzel's field strength (Fs), where the Fs of Al^{3+} = 0.84 Å^{-2}, Si^{4+} = 1.56 Å^{-2}, and S^{6+} = 2.60 Å^{-2}. Accordingly, mullite in contact with SO_x gas implies a higher ΔFs and thus a higher tendency of new phase formation between Al^{3+} and S^{6+} (1.76) than between Si^{4+} and S^{6+} (1.04). This confirms the strong affinity between aluminium and sulphur which consequently results in the formation of the observed aluminium sulphate. As silicon within the mullite has a lower affinity for sulphur it remains as SiO_2 relics (e.g., Figure 4f).

Figure 7.

(a) computed phase stabilities of 1 mole $Al_2(SO_4)_3$ over the temperature range of 300–1000 °C. (b) delta $G0$ calculations for the reactions $Al_2(SO_4)_3 \rightarrow Al_2O_3 + 3\ SO_3$ and $Al_2(SO_4)_3 \rightarrow Al_2O_3 + 3\ SO_2 + 1.5\ O_2$ from 300–1000 °C. (c) computed phase stabilities of 1 mole $Al_6Si_2O_{13}$ and 9 mole SO_3 over the temperature range of 300–1000 °C. (d) delta $G0$ calculations for the reactions $Al_6Si_2O_{13} + 9\ SO_3 \rightarrow 3\ Al_2(SO_4)_3 + 2\ SiO_2$ and $Al_6Si_2O_{13} + 9\ SO_2 + 4.5\ O_2 \rightarrow 3\ Al_2(SO_4)_3 + 2\ SiO_2$ from 300–1000 °C.
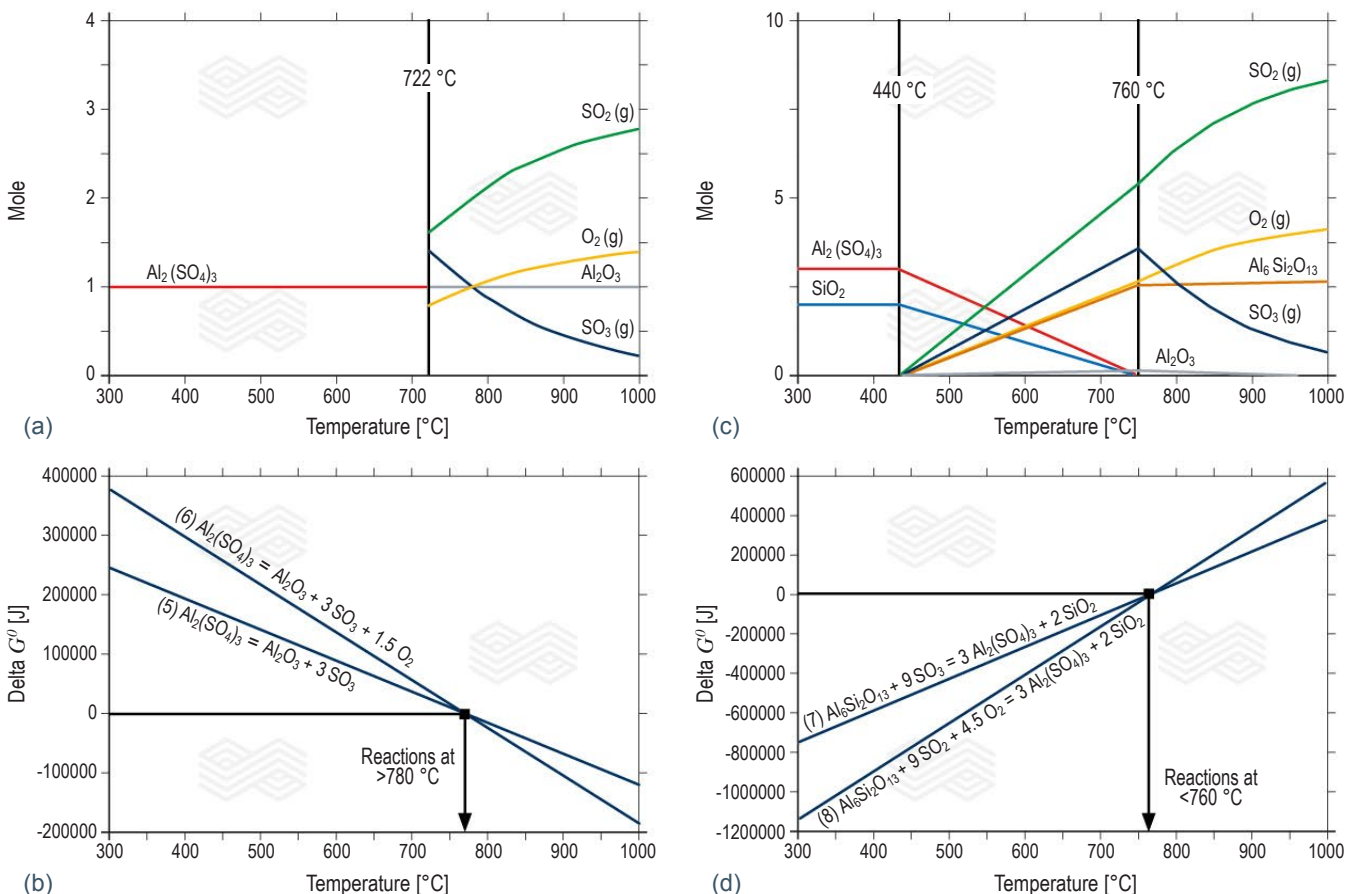
Conclusion

During calcination of hydrated TiO_2 at about 850–950 °C, fireclay bricks in the rotary kiln are affected by a pronounced thermochemical load. Acidic gaseous SO_x attack induces microtextural alteration of the brick matrix up to a depth of ~28 mm from the immediate hot face. This leads to a weakening of the brick bonding structure and enables subsequent discontinuous material loss at the refractory hot face by abrasive wear during the feed material transport through the rotary kiln. Weakening of the brick bonding structure is caused by a two-step corrosion that can be summarised as follows:

- Initially, the supply of gaseous SO_2 and SO_3 into the hot face of the Al_2O_3-SiO_2 brick alters the mullite dominated matrix up to a depth of ~28 mm through equations 7 and 8. Based on thermochemical calculations, mullite in the matrix decomposes to form aluminium sulphate and quartz at temperatures between 760–440 °C. SiO_2 is totally displaced from the matrix and concentrates on the rim areas of large fireclay grains through diffusional processes.
- In a second step, the newly formed aluminium sulphate within the altered brick matrix at the very hot face, up to ~10 mm depth, decomposes at a minimum of 720–780 °C through SO_x gas generation (equations 5 and 6). This temperature estimation is obtained by the combined application of thermochemical phase equilibrium and reaction delta G^0 calculations. Consequently, a very porous and fragile corundum dominated brick matrix is formed that increases the refractory vulnerability against discontinuous material loss by abrasive wear.

The detailed microtextural observations in combination with phase equilibrium modelling and application of the Dietzel's field strength provide evidence that Al_2O_3 in the mullite of the used fireclay bricks strongly interacts with SO_x gas that leads to a significant alteration and weakening of the matrix bonding structure and consequent wear. In contrast, the more acidic SiO_2 species in the brick is widely unaffected by the presence of SO_x gas. Thus, it is recommended to impregnate the bricks with a special silica sol to improve the resistance of the brick matrix against volatile acidic SO_x gas attack.

References

[1] Dietzel, A. Die Kationenfeldstärke und ihre Beziehungen zu Entglasungsvorgängen, zur Verbindungsbildung und zu den Schmelzpunkten von Silikaten. *Zeitschrift für Elektrochemie und angewandte physikalische Chemie*. 1942, 48, 9–23.

[2] Baxter, J.L. Heavy Mineral Sand Deposits of Western Australia. *M.R. Bulletin. Geological Survey of Australia*. 1977, 10, 147.

[3] Chernet, T. Applied Mineralogical Studies on Australian Sand Ilmenite Concentrate With Special Reference to its Behaviour in the Sulphate Process. *Minerals Engineering*. 1999, 12, 485–495.

[4] Lynd, L.E. and Lefond, S.J. *Titanium Minerals. In: Industrial Minerals and Rocks*; Society of Mining Engineers: New York, 1983, 1303–1362.

[5] Stanaway, K.J. Overview of Titanium Dioxide Feedstocks. *Mining Engineering*. 1994, 46, 1367–1370.

[6] Bale, C.W., Bélisle, E., Chartrand, P., Decterov, S.A., Eriksson, G., Gheribi, A.E., Hack, K., Jung, I.-H., Kang, Y.-B., Melançon, J., Pelton, A.D., Petersen, S., Robelin C., Sangster, J., Spencer, P. and Van Ende, M-A. FactSage Thermochemical Software and Databases, 2010–2016. *Calphad*. 2016, 54, 35–53.

[7] Bale, C.W., Chartrand, P., Degterov, S.A., Eriksson, G., Hack, K., Ben Mahfoud, R., Melançon, J., Pelton, A.D. and Petersen, S. FactSage Thermochemical Software and Databases. *Calphad*. 2002, 26, 189–228.

[8] Dietzel, A. Glasstruktur und Glaseigenschaften. *Glastechnische Berichte*. 1948, 22, 41–50, 81–86, 212–224.

Authors

Philip Schantl, RHI Magnesita, Leoben, Austria.
Christian Majcenovic, RHI Magnesita, Leoben, Austria.
Corresponding author: Philip Schantl, Philip.Schantl@rhimagnesita.com